Efficient absorption of visible radiation by gap plasmon resonators

Michael G. Nielsen,[1,*] Anders Pors,[2] Ole Albrektsen,[1] and Sergey I. Bozhevolnyi[1]

[1]*Institute of Technology and Innovation (ITI), University of Southern Denmark, Niels Bohrs Allé 1, DK-5230 Odense M, Denmark*
[2]*Mads Clausen Institute (MCI), University of Southern Denmark, Alsion 2, DK-6400 Sønderborg, Denmark*
[*]*mgni@iti.sdu.dk*

Abstract: We demonstrate experimentally a periodic array of differently-sized and circularly-shaped gap plasmon resonators (GPRs) with the average absorption ~94% for unpolarized light in the entire visible wavelength range (400-750nm). Finite-element simulations verify that the polarization insensitive broadband absorption originates from localized gap surface plasmons whose resonant excitations only weakly depend on the angle of incidence. Arrays of GPRs also exhibit enhanced local field intensities (~115) as revealed by scanning two-photon photoluminescence microscopy, that are spectrally correlated with the minima in corresponding linear reflection spectra.

References and links

1. J. A. Schuller, E. S. Barnard, W. Cai, Y. C. Jun, J. S. White, and M. L. Brongersma, "Plasmonics for extreme light concentration and manipulation," Nat. Mater. **9**(3), 193–204 (2010).
2. J. N. Anker, W. P. Hall, O. Lyandres, N. C. Shah, J. Zhao, and R. P. Van Duyne, "Biosensing with plasmonic nanosensors," Nat. Mater. **7**(6), 442–453 (2008).
3. H. Liu, L. Zhang, X. Lang, Y. Yamaguchi, H. Iwasaki, Y. Inouye, Q. Xue, and M. Chen, "Single molecule detection from a large-scale SERS-active Au79AG21 substrate," Nat. Sci. Rep. **1**, 1–5 (2011).
4. H. A. Atwater and A. Polman, "Plasmonics for improved photovoltaic devices," Nat. Mater. **9**(3), 205–213 (2010).
5. V. E. Ferry, A. Polman, and H. A. Atwater, "Modeling light trapping in nanostructured solar cells," ACS Nano **5**(12), 10055–10064 (2011).
6. Y. Wang, T. Sun, T. Paudel, Y. Zhang, Z. Ren, and K. Kempa, "Metamaterial-plasmonic absorber structure for high efficiency amorphous silicon solar cells," Nano Lett. **12**(1), 440–445 (2012).
7. K. Aydin, V. E. Ferry, R. M. Briggs, and H. A. Atwater, "Broadband polarization-independent resonant light absorption using ultrathin plasmonic super absorbers," Nat Commun. **2**, 517 (2011).
8. J. Hao, J. Wang, X. Liu, W. J. Padilla, L. Zhou, and M. Qiu, "High performance optical absorber based on a plasmonic metamaterial," Appl. Phys. Lett. **96**(25), 251104 (2010).
9. N. Liu, M. Mesch, T. Weiss, M. Hentschel, and H. Giessen, "Infrared perfect absorber and its application as plasmonic sensor," Nano Lett. **10**(7), 2342–2348 (2010).
10. J. Hao, L. Zhou, and M. Qiu, "Nearly total absorption of light and heat generation by plasmonic metamaterials," Phys. Rev. B **83**(16), 165107 (2011).
11. S. Chen, H. Cheng, H. Yang, J. Li, X. Duan, C. Gu, and J. Tian, "Polarization insensitive and omnidirectional broadband near perfect planar metamaterial absorber in the near infrared regime," Appl. Phys. Lett. **99**(25), 253104 (2011).
12. A. Tittl, P. Mai, R. Taubert, D. Dregely, N. Liu, and H. Giessen, "Palladium-based plasmonic perfect absorber in the visible wavelength range and its application to hydrogen sensing," Nano Lett. **11**(10), 4366–4369 (2011).
13. J. Le Perchec, Y. Desieres, N. Rochat, and R. Espiau de Lamaestre, "Subwavelength optical absorber with an integrated photon sorter," Appl. Phys. Lett. **100**(11), 113305 (2012).
14. M. G. Nielsen, D. K. Gramotnev, A. Pors, O. Albrektsen, and S. I. Bozhevolnyi, "Continuous layer gap plasmon resonators," Opt. Express **19**(20), 19310–19322 (2011).
15. S. I. Bozhevolnyi and T. Søndergaard, "General properties of slow-plasmon resonant nanostructures: nano-antennas and resonators," Opt. Express **15**(17), 10869–10877 (2007).
16. J. Jung, T. Søndergaard, and S. I. Bozhevolnyi, "Gap plasmon-polariton nanoresonators: scattering enhancement and launching of surface plasmon polaritons," Phys. Rev. B **79**(3), 035401 (2009).
17. T. Søndergaard, J. Jung, S. I. Bozhevolnyi, and G. Della Valle, "Theoretical analysis of gold nano-strip gap plasmon resonators," New J. Phys. **10**(10), 105008 (2008).

18. T. Søndergaard, S. I. Bozhevolnyi, J. Beermann, S. M. Novikov, E. Devaux, and T. W. Ebbesen, "Resonant plasmon nanofocusing by closed tapered gaps," Nano Lett. **10**(1), 291–295 (2010).
19. T. Søndergaard, S. I. Bozhevolnyi, S. M. Novikov, J. Beermann, E. Devaux, and T. W. Ebbesen, "Extraordinary optical transmission enhanced by nanofocusing," Nano Lett. **10**(8), 3123–3128 (2010).
20. V. G. Kravets, F. Schedin, and A. N. Grigorenko, "Plasmonic blackbody: almost complete absorption of light in nanostructured metallic coatings," Phys. Rev. B **78**(20), 205405 (2008).
21. M. K. Hedayati, M. Javaherirahim, B. Mozooni, R. Abdelaziz, A. Tavassolizadeh, V. S. K. Chakravadhanula, V. Zaporojtchenko, T. Strunkus, F. Faupel, and M. Elbahri, "Design of a perfect black absorber at visible frequencies using plasmonic metamaterials," Adv. Mater. (Deerfield Beach Fla.) **23**(45), 5410–5414 (2011).
22. P. Bouchon, C. Koechlin, F. Pardo, R. Haïdar, and J.-L. Pelouard, "Wideband omnidirectional infrared absorber with a patchwork of plasmonic nanoantennas," Opt. Lett. **37**(6), 1038–1040 (2012).
23. Y. Cui, K. H. Fung, J. Xu, H. Ma, Y. Jin, S. He, and N. X. Fang, "Ultrabroadband light absorption by a sawtooth anisotropic metamaterial slab," Nano Lett. **12**(3), 1443–1447 (2012).
24. P. B. Johnson and R. W. Christy, "Optical constants of the noble metals," Phys. Rev. B **6**(12), 4370–4379 (1972).
25. S. Zhang, W. Fan, K. J. Malloy, S. R. J. Brueck, N. C. Panoiu, and R. M. Osgood, "Demonstration of metal-dielectric negative index metamaterials with improved performance at optical frequencies," J. Opt. Soc. Am. B **23**(3), 434–438 (2006).
26. P. J. Schuck, D. P. Fromm, A. Sundaramurthy, G. S. Kino, and W. E. Moerner, "Improving the mismatch between light and nanoscale objects with gold bowtie nanoantennas," Phys. Rev. Lett. **94**(1), 017402 (2005).
27. J. Beermann, S. M. Novikov, T. Søndergaard, A. Boltasseva, and S. I. Bozhevolnyi, "Two-photon mapping of localized field enhancements in thin nanostrip antennas," Opt. Express **16**(22), 17302–17309 (2008).
28. M. G. Nielsen, A. Pors, R. B. Nielsen, A. Boltasseva, O. Albrektsen, and S. I. Bozhevolnyi, "Demonstration of scattering suppression in retardation-based plasmonic nanoantennas," Opt. Express **18**(14), 14802–14811 (2010).

1. Introduction

Subwavelength noble metal nanostructures supporting localized surface plasmons (LSPs) and propagating surface plasmon polaritons (SPPs) have attracted great interest due to their unique abilities of enhancing electromagnetic fields and confining light to the nanometer-scale in the visible and near-infrared wavelength range [1]. The corresponding resonances, manifested by enhanced absorption- and scattering cross sections, have lead to many exciting applications such as nanoscale environmental sensing [2] and surface-enhanced Raman scattering (SERS) from individual molecules [3]. Recently plasmonics has also gained increased attention in the field of photovoltaics for realizing ultrathin solar cells with improved efficiencies by tailoring noble metal nanoparticles and sub-micrometer thin films for optimizing light absorption in silicon [4–6].

Recent studies have shown that layered metal/dielectric/metal nanostructures with only the top metal layer lithographically patterned are excellent plasmonic absorbers in the visible [7] and especially in the near-infrared [8–13]. Such nanostructures can be considered as continuous layer gap plasmon resonators (CL-GPRs) [14], where the electromagnetic field is highly concentrated in the dielectric gap due to constructively interfering gap plasmons which are efficiently reflected at the resonator terminations [14–19]. The gap plasmon resonance wavelength is therefore easily controlled by modifying the nanostructure dimensions and/or the dielectric layer thickness [14]. Although significant broadband absorption has been achieved in the visible by exploiting one dimensional deep gold composite diffraction gratings [20] or nearly percolated metal/dielectric nanocomposites [21], the realization of a two dimensional broadband absorber in the visible with discrete plasmonic components in periodically arranged unit-cells that are smaller than the free-space wavelength does, however, pose a formidable challenge. Recent publications have shown that even in the infrared, the achievable broadband response may exhibit significant oscillations with reflectivities as large as ~0.5 in the wavelength range of interest [22], or rely on utilizing multiple layered anisotropic metamaterials [23].

In this work, we demonstrate a polarization insensitive CL-GPR array with ~0.94 average measured absorption in the entire visible spectrum 400-750nm. The CL-GPR unit-cell consists of various-sized gold nanoparticles on top of a continuous ~20nm thin SiO_2 layer which is supported by a 100nm thick gold film. We also demonstrate that a CL-GPR array with ~0.89 average measured absorption can be achieved in the wavelength range 400-850nm simply by tuning and combining various gold nanoparticle diameters. Finally, we investigate the CL-GPR intensity enhancements as function of the wavelength in the near-infrared via

scanning two-photon photoluminescence (TPL) microscopy, and verify that the intensity enhancements are spectrally correlated with minima in corresponding linear reflection spectra.

2. Reflection measurements and simulations

In analogy with a standard Fabry-Perot resonator, individual CL-GPRs can be tuned to resonantly enhance light by controlling the length of the particle (resonator) situated above the dielectric film. Importantly, for very thin dielectric films the light is efficiently concentrated and eventually absorbed in the CL-GPRs due to the large gap plasmon effective index [14]. Circularly-shaped CL-GPRs therefore allow for efficient polarization insensitive absorption which can be spectrally tuned via the particle diameter.

The CL-GPR resonance wavelength λ is related to the particle diameter d by [14]

$$d \frac{2\pi}{\lambda} n_{gsp} = m\pi - \varphi, \tag{1}$$

where n_{gsp} is the gap plasmon effective index, m is an integer representing the gap plasmon mode order and φ the phase acquired upon reflection from the resonator terminations [14]. As a starting point for obtaining polarization insensitive absorption in the entire visible spectrum, we therefore fabricate unit-cells comprising four CL-GPRs where the gold nanoparticles above the dielectric film are circular symmetric and with variable diameters [Fig. 1(a)]. The base substrate is a silicon wafer onto which a 100nm thick gold film is deposited by electron-beam evaporation followed by deposition of a ~20nm SiO_2 thin film by RF-sputtering. Subsequently, the sample is lithographically structured with gold nanoparticles in a ~30μm × 30μm array by electron-beam lithography and liftoff which is applied to a 50nm thick gold film deposited by electron-beam evaporation [Fig. 1(b), 1(c)]. In order to minimize the influence of diffraction effects in the visible wavelength range, the unit-cell size is chosen to Λ = 340nm (170nm particle period) and is therefore smaller than the shortest free-space wavelength 400nm. Based on Eq. (1), setting $m = 1$ and $\varphi = 0$, and the calculated gap plasmon effective indexes 3.95, 3.54, 3.15 and 3.00, corresponding to resonance wavelengths ~550, ~600, ~675 and ~750 nm, respectively, we choose $d_1 = 60$nm, $d_2 = 80$nm, $d_3 = 100$nm and d_4 = 120nm in order to achieve absorption in a broad spectral range in the visible. The CL-GPR reflection phase φ is undoubtedly larger than zero [14], however, due to small uncertainties in the structural parameters and the roughness of nanoparticle edges the exact value of φ is difficult to estimate precisely and as an initial guess for the design we therefore set $\varphi = 0$.

For the purpose of estimating the absorption of the fabricated sample, we conduct reflection measurements where light from a broadband halogen light source is focused by an objective, having 50x magnification and 0.75 numerical aperture, onto the 30μm × 30μm CL-GPR array. The reflected light is collected by the same objective and spatially filtered so that only light from a circular area (centered on the CL-GPR array) with diameter ~16μm is collected, thereby avoiding reflection from the array edges exhibiting larger reflection due to lithographic proximity effects. Finally the reflected light is guided via an optical fiber to a VIS/NIR spectrometer which is operated with 100ms integration time and averaging 50 spectra, and the array reflection spectra are normalized with a reflection spectrum collected on
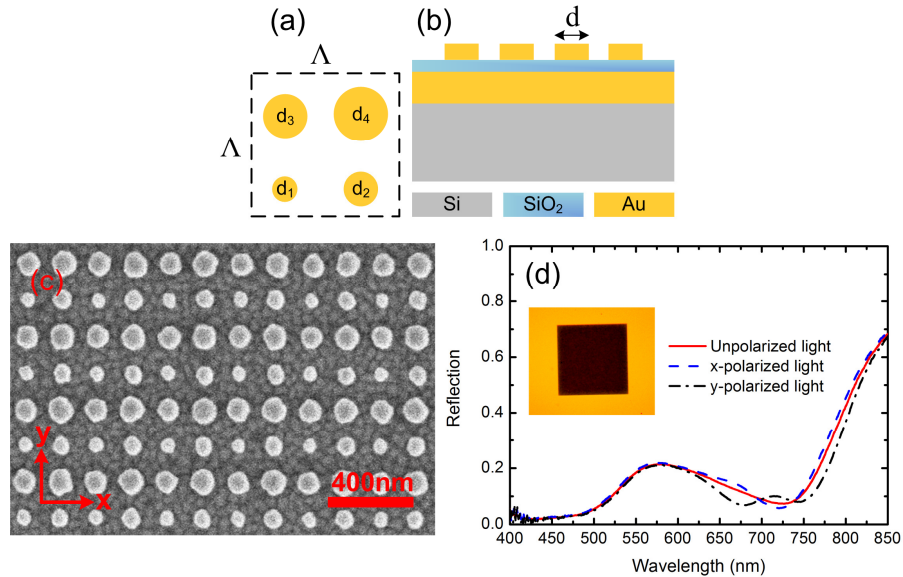
Fig. 1. (a) Schematic representation of the quadratic unit-cell of size Λ, and containing four gold nanoparticles with different diameters d. (b) Schematic representation of the layered sample structure. (c) SEM-image of the fabricated CL-GPRs with particle diameters d_1 = 60nm, d_2 = 80nm, d_3 = 100nm and d_4 = 120nm and unit-cell size Λ = 340nm. (d) Reflection spectra for unpolarized (solid red curve), x-polarized (dashed blue curve) and y-polarized (black dash-dotted curve) light. The inset shows a microscope image of the 30μm × 30μm CL-GPR array for unpolarized light and its appearance compared to the surrounding smooth gold film coated with ~20nm SiO₂.

a laser mirror silver reference (Edmund optics, NT64-114) with an average reflection of 99% between 350 and 1100nm [Fig. 1(d)].

The array appear quite dark compared to the surrounding smooth gold/SiO₂ film [inset in Fig. 1(d)] and for wavelengths shorter than ~750nm the reflection is less than ~0.2 except in a small wavelength range centered at ~570nm. It is also interesting that the reflection is less than ~0.1 for wavelengths shorter than ~525nm, however, this is mainly attributed to the increasing intrinsic losses in gold for wavelengths shorter than ~525nm resulting in strong absorption of the scattered electromagnetic fields within the CL-GPR array.

The reflection is measured with unpolarized light (red solid curve), x-polarized light (blue dashed curve) and y-polarized light (black dash-dotted curve), showing basically the same features of low reflection due to the circular symmetry of the gold nanoparticles. There is, however, a slight difference in the reflection spectra fine structure in the wavelength range ~650-750nm, which is due to the unit-cell asymmetry w.r.t. the nanoparticle diameter and fabrication imperfections. As expected the reflection spectrum recorded with unpolarized light is an approximate average of the spectra recorded with x- and y-polarized light and the features appearing in spectra obtained with polarized light at wavelengths ~650-750nm are therefore not seen in spectra obtained with unpolarized light. Since the 100nm thickness of the gold substrate is substantially larger than the skin depth in gold there is no transmission and the absorption A can be estimated directly from the reflection R as $A = 1-R$ resulting in an average measured absorption of ~0.89 in the wavelength range 400-750nm.
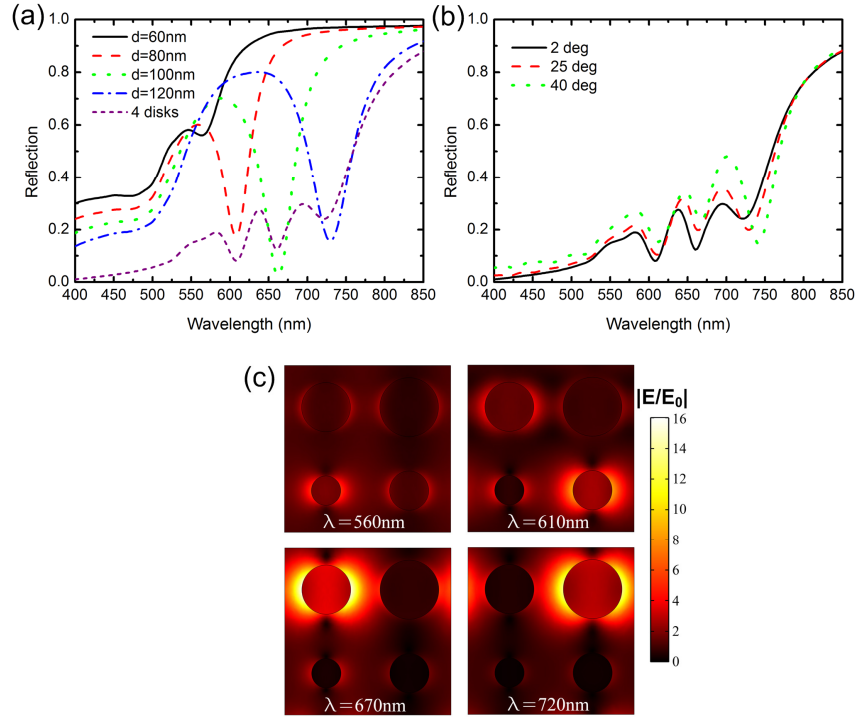
Fig. 2. (a) Simulated reflection spectra for unit-cells with a single CL-GPR and for the unit-cell containing four particles (purple dashed curve) when exciting with an x-polarized plane wave at normal incidence. (b) Simulated reflection spectra averaged for x- and y- polarized light, respectively, for incidence angles 2, 25 and 40 degrees. (c) Simulated electric field enhancement maps for x-polarized light showing that the gap plasmons in the four particles with diameters d = 60, 80, 100 and 120nm are individually excited at wavelengths λ = 560, 610, 670 and 720nm, respectively. The maps are plotted in a plane through the CL-GPRs 25nm above the SiO₂ film.

In order to verify that the low reflection is due to gap plasmons excited in the individual CL-GPRs we have conducted 3D simulations with the finite element method (FEM) via the software package COMSOL Multiphysics in order to simulate the far- and near-field optical response of the CL-GPRs. In the FEM simulations, the SiO₂ layer thickness and gold disk thickness are 20nm and 50nm, respectively, i.e. the unit-cells are identical to those in the experiment, but without the supporting silicon substrate. The periodicity is established by Floquet boundary conditions on the unit-cell side walls and the dielectric response of gold is incorporated in the model via interpolation of tabulated optical constants [24] and the refractive index of SiO₂ is set to n_{SiO2} = 1.45.

As a first approach we calculate the reflection spectra, normalized with the intensity of the incident light, from unit-cells occupying a single CL-GPR with diameters 60, 80, 100 and 120nm and which are excited with a normally incident x-polarized plane wave [Fig. 2(a)]. The spectra exhibit pronounced plasmonic resonances at wavelengths 560, 610, 670, and 730nm and as expected the plasmonic resonances are redshifted when the particle diameter is increased. Particularly, the resonance wavelengths can be predicted by Eq. (1) when setting the average reflection phase φ = 0.29 and m = 1, however, with a worst case error of ~15%. For the fixed unit-cell size Λ = 340nm the reflection level at resonance strongly depends on the diameter d and has a minimum for d = 100nm where the reflection is nearly zero. In other words, when the nanoparticle fill factor is gradually increased the reflection correspondingly drops down until a certain fill factor threshold is reached, and above this threshold two mechanisms result in increased reflection. As the nanoparticle diameter increases the first mechanism that comes into play is the overlapping mode volume of neighboring nanoparticles

which reduces the gap plasmon excitation efficiency due to the subwavelength distance between particle edges. The second mechanism, important for even larger diameters, is the gap plasmon near-field coupling which affects both the excitation efficiency and the resonance wavelength.

Calculation of the reflection spectrum for the unit-cell comprising all four CL-GPRs [purple dashed curve in Fig. 2(a)] reveals reflection minima which are directly comparable with the resonances of the individual CL-GPRs and indicates reflections below ~0.25 in the visible spectrum. The CL-GPRs are therefore not coupled to each other via their near-fields, however, due to the mentioned subwavelength distance between the nanoparticle edges the achieved reflection at wavelengths 670nm and 730nm is slightly larger compared to in the situation where there is just one nanoparticle occupying the unit-cell. We note that the experimentally estimated reflection is slightly lower than the simulated reflection in the wavelength range ~650-750nm [compare Fig. 1(d) and Fig. 2(a) purple dashed curve], but this is very likely due to the gold nanoparticle surface scattering and grain boundary effects resulting in a larger damping constant of the gold nanoparticles compared to that of bulk gold [9,25]. Apart from this observation the experimental and simulated reflection spectra basically show the same trends.

In order to investigate the reflection dependence on the angle of incidence and polarization state of the incident light, we simulate the reflection of the unit-cell comprising the four CL-GPR for incidence angles 2, 25 and 40 degrees averaged for x- and y-polarized plane wave excitations [Fig. 2(b)], respectively. For incidence angles smaller than 25 degrees the reflection spectrum is basically unchanged and for larger angles the average reflection only increases slightly. The low reflection can therefore be achieved for a large range of incident angles and, importantly, the reflection resonances are spectrally quite insensitive w.r.t. the angle of incidence and the polarization state, which confirms that the low reflection is not due to periodic effects, but related to localized gap plasmon resonances. This is also demonstrated by plotting the electric field enhancement in a plane through the CL-GPRs 25nm above the SiO_2 layer for the case of a normally incident x-polarized plane wave [Fig. 2(c)], which clearly shows that the observed reflection resonances are correlated with resonant field enhancements in the individual CL-GPRs

Based on the simulated reflection spectra [Fig. 2(a)], a larger reflection seen in the experimental reflection spectra at wavelengths near ~570nm [Fig. 1(d)] can be explained by a smaller fill factor related to the smallest particle with diameter $d_1 = 60$nm compared to the three larger ones. In order to obtain lower reflection, and thereby larger absorption, in the entire visible wavelength range, additional small particles must therefore be added to the CL-GPR unit-cell. In order to ensure that the gold nanoparticles are not short-circuited due to electron-beam overexposure, the position of the particles with diameter $d_1 = 60$nm and $d_3 = 100$nm are interchanged. Hereafter nine additional particles with diameter ~55nm are introduced into the unit-cell [Fig. 3(a)] resulting in the fill factor increasing from ~0.23 to ~0.33. The fabricated 30μm × 30μm CL-GPR array [Fig. 3(b)] is visually black [inset in Fig. 3(c)] and the average measured absorption is now ~0.94 in the wavelength range 400-750nm, which is a significant improvement compared to a recently suggested periodically arranged plasmonic super absorber [7], and close to the average measured absorption recently achieved with metal/dielectric nanocomposites [21]. We also measured the reflection when using an objective with 100x magnification and 0.90 numerical aperture in order to verify the negligible angle of incidence dependence. In this case the spectra did not change except for a slight increase in reflection in the wavelength range 400-500nm (not shown) resulting in an average measured absorption of ~0.92 for wavelengths 400-750nm.

Clearly the reflection increases rapidly for wavelengths longer than ~750nm [Fig. 3(c)] and in order to reduce the reflection in the near-infrared as well it is necessary to introduce larger nanoparticles in the unit-cell which resonates at longer wavelengths. The increased nanoparticle diameters when the unit-cell size is $Λ = 340$nm lead to short-circuited particles
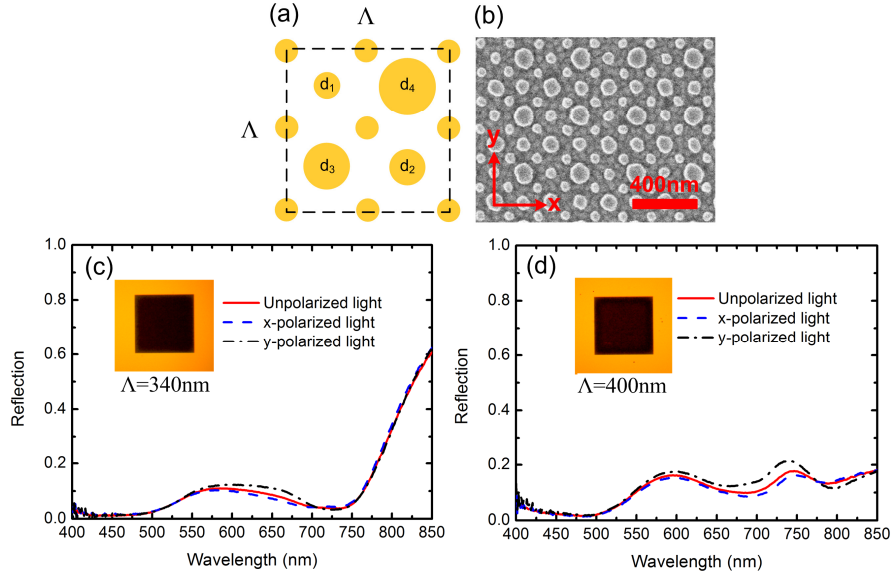
Fig. 3. (a) Schematic representation of the unit-cell comprising four gold nanoparticles with different diameters and nine additional small gold nanoparticles with identical diameter. The unit-cell size is Λ = 340nm. (b) SEM-image of the fabricated CL-GPRs with particle diameters d_1 = 60nm, d_2 = 80nm, d_3 = 100nm and d_4 = 120nm and nine additional particles with diameter 55nm. (c) Reflection spectra for unpolarized (solid red curve), x-polarized (dashed blue curve) and y-polarized (black dash-dotted curve) light. The inset shows a microscope image of the 30μm × 30μm patterned area and its appearance compared to the smooth surrounding gold film coated with ~20nm SiO$_2$. (d) Reflection spectra of a similar CL-GPR array, but with unit-cell size Λ = 400nm and particle diameters d_1 = 90nm, d_2 = 115nm, d_3 = 125nm and d_4 = 160nm. The nine additional particles have diameter 75nm.

and the unit-cell size is consequently increased to Λ = 400nm. Increasing hereafter the nanoparticle diameters in the unit-cell to d_1 = 90nm, d_2 = 115nm, d_3 = 125nm and d_4 = 160nm, and including the nine additional particles having diameter 75nm, results in a fill factor of ~0.43 and average measured absorption of ~0.89 in the wavelength range 400-850nm [Fig. 3(d)]. We hereby conclude that it is possible to realize polarization insensitive plasmonic broadband absorbers in the visible *and* near-infrared by virtue of CL-GPRs.

3. Estimation of intensity enhancements by two-photon photoluminescence microscopy

The low reflection inside the CL-GPR array [inset of Fig. 3(c)] is an indication of strongly enhanced local fields which are eventually absorbed in the gold. We use scanning TPL microscopy in order to estimate the intensity enhancement factor $\alpha(\lambda)$ in the CL-GPR array relative the intensity enhancement from a smooth gold reference. TPL is extremely sensitive to intense local fields due its quadratic intensity dependence, and we estimate the intensity enhancement factor $\alpha(\lambda)$ via the following relation [26]:

$$\frac{TPL_{array}}{TPL_{ref}} = \alpha(\lambda) \frac{\langle P_{array} \rangle^2 A_{array}}{\langle P_{ref} \rangle^2 A_{ref}}, \tag{2}$$

where *TPL* is the obtained TPL signal, $\langle P \rangle$ is the used average incident power from a mode-locked titanium-sapphire laser (200fs pulse duration and 80MHz repetition rate) which is tunable within the wavelength ~730-850nm, and *A* is the area generating the TPL signal. As a first approximation we assume that the TPL generating areas are the same A_{array} = A_{ref}

meaning that $\alpha(\lambda)$ is an average and slightly underestimated intensity enhancement factor [14]. In Eq. (2) it is also assumed that the size of the laser spot, which is focused with an objective
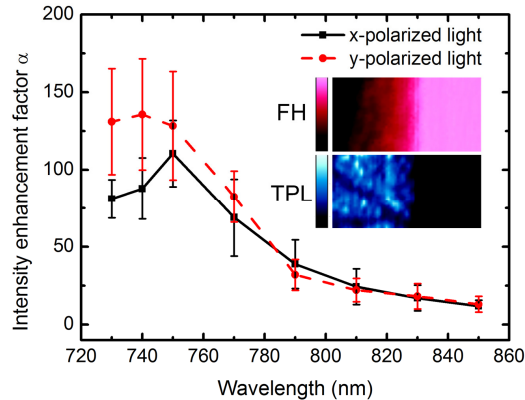

Fig. 4. Intensity enhancement factor $\alpha(\lambda)$ as a function of the wavelength for x-polarized light (black solid curve) and y-polarized light (red dashed curve) of the sample shown in [Fig. 3(c)]. The insets show 10μm × 5μm scanned areas across the array boundary where FH (upper red) and TPL (lower blue) is measured at the free-space wavelength 750nm.

with 100x magnification and 0.70 numerical aperture, is the same when focusing on the CL-GPR array and on the reference, and furthermore that the reference, which is a 50nm thick smooth gold film lithographically defined nearby the CL-GPR array, is not enhancing the local fields. The TPL-setup has previously been described in detail [27, 28] and we have shown that the intensity enhancement factor $\alpha(\lambda)$ is correlated to minima in reflection spectra and is an informative measure of plasmonic resonance strengths.

By scanning areas of 10μm × 5μm and collecting concurrently the reflected first-harmonic (FH) and TPL (upper red and lower blue insets in Fig. 4, respectively), we conduct relative TPL measurements for wavelengths 730-850nm. The quadratic dependence of the TPL signal on the incident intensity was verified when measuring in the CL-GPR array as well as on the gold reference by varying the incident power at a fixed wavelength 770nm (not shown). The estimated intensity enhancement factors $\alpha(\lambda)$ (Fig. 4) are well correlated with the reflection minimum at wavelength ~740nm [Fig. 3(c)] since the enhancement is largest (~115 on average) for wavelengths 730-750nm and strongly decreasing (approaching one) for longer wavelengths. For wavelengths shorter than ~750nm the average intensity enhancement factors $\alpha(\lambda)$ for x- and y-polarized light, respectively, are slightly deviating. This is in the wavelength range of most intense local fields and therefore also the wavelength range where the intensity enhancement is most sensitive to experimental uncertainties and taking this into account the intensity enhancement factor trends are quite similar for x- and y-polarized light. Significant intensity enhancements are therefore achievable regardless of the incident light polarization.

4. Conclusion

In conclusion, it has been demonstrated experimentally and verified by FEM simulations that arrays of differently-sized and circularly-shaped CL-GPRs can serve as polarization insensitive broadband super absorbers in the visible. Using reflection spectroscopy, we have shown that CL-GPR arrays can exhibit ~0.94 and ~0.89 average measured absorption in the wavelength regimes 400-750nm and 400-850nm, respectively. It has also been demonstrated experimentally by scanning TPL microscopy that a CL-GPR array locally enhances electric field intensities more than 100 times regardless of the incident light polarization and we envision that such arrays can have profound applications in single molecule SERS and in the realization of ultrathin highly absorbing photovoltaic devices where the SiO_2 layer is replaced by an active semiconductor.

Acknowledgments